Thermoacoustic modes of intrinsic and acoustic origin and their interplay with exceptional points

Alessandro Orchini[a,*], Camilo F. Silva[b], Georg A. Mensah[c], Jonas P. Moeck[d]

[a]*Institut für Strömungsmechanik und Technische Akustik, Technische Universität Berlin, Berlin, Germany*
[b]*Fakultät für Maschinenwesen, Technische Universität München, Garching, Germany*
[c]*CAPS Laboratory, Department of Mechanical and Process Engineering, ETH Zürich, Zurich Switzerland*
[d]*Department of Energy and Process Engineering, Norwegian University of Science and Technology, Trondheim, Norway*

Abstract

We propose a general classification of all the modes of a given thermoacoustic system into two sets: one of acoustic origin and one of intrinsic thermoacoustic (ITA) origin. To do this, the definition of intrinsic modes, traditionally based on anechoic boundary conditions, is reformulated in terms of the gain n of the Flame Transfer Function (FTF). As a consequence of this classification, we show how theoretical results for the estimation of all thermoacoustic modes can be derived in the limit $n \to 0$, for both axial and annular combustors, independent of the acoustic boundary conditions. Starting from this limit and using standard continuation methods while increasing n, all the eigenvalues of interest in a given domain in the frequency space can be identified. We also discuss how thermoacoustic modes of acoustic and ITA origin can interact, and in some cases coalesce generating exceptional points (EPs).

*Corresponding Author
Email address: a.orchini@campus.tu-berlin.de (Alessandro Orchini)

Although all EPs found have negative growth rates, in their vicinity thermoacoustic eigenmodes have very large sensitivities and exhibit strong mode veering. We demonstrate how, in some cases, mode veering is responsible for the occurence of thermoacoustic instabilities, and propose a numerical method to identify EPs. All the theoretical results are numerically verified using two generic thermoacoustic configurations.

Keywords: Thermoacoustics, Intrinsic modes, Exceptional point, Combustion instabilities

---

1. Introduction

Intrinsic thermoacoustic (ITA) instabilities were first recognized in [1, 2], where it was shown that even a thermoacoustic system with anechoic boundary conditions can exhibit thermoacoustic instabilities. Analytical models of ITA instabilities were developed in [3, 4], which allowed for their connection to an intrinsic feedback loop that does not require acoustic reflections at boundaries. Using an n–τ model, it was shown that the ITA resonance frequency can be calculated from the time delay of the acoustic flame response only, and that ITA resonance frequencies are directly related to the peaks of the elements of the scattering matrix [5, 6].

Direct numerical simulations of anechoic systems that exhibited ITA instabilities [7, 8], together with some experimental evidence [2, 9], further corroborate that ITA instabilities are indeed physical, and not just the result of a mathematical artifact. The physical mechanism governing ITA instabilities relies on the feedback between acoustic waves generated by unsteady heat release rate and the latter being sensitive to acoustic velocity fluctuations upstream of the flame [10, 11]. ITA instabilities do not require ideal anechoic conditions to exist: in [12, 13] it has been demonstrated that this kind of instability is relevant in thermoacoustic systems with partially reflecting boundary conditions. In [14] it was shown that, for a fully reflective Rijke-tube like systems with an n–τ flame response model, the resonance frequency characterizing the ITA feedback loop for $n \to 0$ is the same as the one obtained in anechoic systems. In [15] the evolution of thermoacoustic eigenfrequency trajectories from fully reflecting to anechoic conditions was reported. Some trajectories are pushed to infinitely negative growth rates in the anechoic limit, others retain a finite frequency and growth rate. The former were called ITA eigenfrequencies (for nonzero reflecting conditions) and the latter "pure ITA" eigenfrequencies (in the anechoic limit).

One objective of the present study is demonstrating that the conclusions derived for ITA modes in simple configurations (straight Rijke tubes) and/or with simple flame models (n–τ) can be generalized to a much larger set of thermoacoustic systems. We will show that a clear distinction between "ITA driven" and "acoustic driven" thermoacoustic modes (as in [15]) is not always possible when using the definitions of ITA and acoustic modes given in the literature; an alternative definition that allows for this distinction is proposed. Furthermore, we will show that the interplay between modes of acoustic and ITA origin leads to the existence of exceptional points (EPs). EPs have been identified as the fundamental concept at the base of many scientific phenomena in several fields, including non-Hermitian quantum mechanics, optics and acoustics [16–18]. In thermoacoustics, they have only been recently discussed [19]. At EPs two or more eigenvalues coalesce and so do their corresponding modeshapes. The resulting eigenvalue is, thus, degenerate and defective. In the simplest case, a defective eigenvalue has algebraic multiplicity two and geometric multiplicity one. This is accompanied by special properties like infinite parameter sensitivity. The effects of EPs on thermoacoustic eigenvalue trajectories is the second main objective of the study. In particular, we will demonstrate how thermoacoustic eigenmodes can become unstable because of strong mode veering caused by their interaction with EPs, even if the latter have negative growth rates. The identification of EPs, thus, helps understanding the origin of some thermoacoustic instabilities.

In §2, the definition of ITA modes is revised, and the findings of [14] are generalized to arbitrary thermoacoustic systems. It is also shown that a given thermoacoustic mode could be thought of as originating from either an acoustic or a "pure ITA" mode, depending on whether a thermoacoustic configuration is considered to be originating from (i) an acoustic cavity in which the strength of the flame is gradually increased, or (ii) an anechoic combustion chamber in which the reflection coefficients are gradually increased. In §3, this ambiguity is tied to the existence of EPs. A general strategy to numerically identify EPs is proposed, and their effect on the trajectories of thermoacoustic modes is discussed. The theory is demonstrated in §4 using two thermoacoustic configurations modeled with the 3D Helmholtz equation. In §4.1 an axial combustor is considered, and EPs stemming from the interaction between acoustic and ITA modes are found; in §4.2 an annular combustor is considered, and an EP is identified as the coalescence of two thermoacoustic modes of acoustic origin.

2. Acoustic, intrinsic, and thermoacoustic modes

Thermoacoustic phenomena arise from the interaction between unsteady heat release rate and acoustic fluctuations. The linear stability of thermoacoustic systems in the low-Mach-number limit can be assessed by investigating the eigenvalues of the Helmholtz equation with a heat release source term [20, 21]. In the frequency domain it reads [22, 23]

$$\nabla \cdot \left(c^2 \nabla \hat{p}\right) - s^2 \hat{p} - \frac{(\gamma - 1)}{\overline{\rho}} \frac{\overline{q}(\boldsymbol{x})}{\overline{u}} \mathcal{F}(s) \nabla \hat{p}_{\mathrm{ref}} \cdot \hat{\boldsymbol{n}}_{\mathrm{ref}} = 0, \tag{1}$$

where $\hat{p}$ represents the pressure fluctuations in frequency domain, γ the heat capacity ratio, c the local speed of sound, $\overline{\rho}$ the mean density, and $s \equiv \sigma + \mathrm{i}\omega$ the Laplace variable – where σ is the growth rate and $\omega \equiv 2\pi f$ is the angular frequency – representing the eigenvalues of interest. $\mathcal{F}(s)$ is the Flame Transfer Function (FTF), which represents the linear response of heat release rate fluctuations resulting from perturbations in the acoustic velocity field at a reference location, indicated with the subscript $()_{\mathrm{ref}}$. The heat release is located only in a (compact) sub-domain of the total volume, where the local mean heat release, $\overline{q}(\boldsymbol{x})$ in Eq. (1), is non-zero. Here we are implicitly assuming that the unsteady heat release rate is proportional to the mean one, which is not strictly necessary but inconsequential due to the acoustic compactness of the flame.

The FTF is often expressed in terms of the n–τ model

$$\mathcal{F}(s) \equiv \frac{\overline{u}}{\overline{Q}} \frac{\hat{q}}{\hat{u}} \equiv n e^{-s\tau}, \tag{2}$$

where n and τ represent the heat release gain and time-lag with respect to velocity fluctuations, and $\overline{u}$ and $\overline{Q}$ are the mean characteristic velocity and mean global heat release rate, respectively. A non-dimensional impedance Z specifies the boundary conditions:

$$\hat{p} + \frac{cZ}{s} \nabla \hat{p} \cdot \hat{\boldsymbol{n}} = 0. \tag{3}$$

Traditionally, thermoacoustic modes have been understood as perturbations of purely acoustic modes (as defined in §1). Consequently, their eigenfrequencies and modeshapes have been sought in the vicinity of those of the same system without any unsteady heat release rate ($\mathcal{F} = 0$ in eq. (1)). By this assumption, Galerkin mode expansions of thermoacoustic modes based on the acoustic modes have been proposed [24]. The recently discovered intrinsic thermoacoustic modes, however, show that this is not always appropriate. Thermoacoustic oscillations can have frequencies which are not directly related to the purely acoustic eigenfrequencies of the combustor [1, 9]. This is because these modes arise from the feedback loop created by upstream traveling acoustic perturbations generated by the flame, which trigger velocity fluctuations upstream of the flame [10, 11, 25]. These in turn lead to the generation of heat release rate fluctuations (see Fig. 2). Because this mechanism does not require any interaction with acoustic waves reflected at the boundaries, its associated modes have been labelled ITA modes.

2.1. Origin of thermoacoustic modes

From the literature, modes of ITA origin are defined to be those associated with the eigenfrequency loci that contain pure ITA eigenfrequencies in the anechoic limit [26]. Equivalently, modes of acoustic origin are defined to be those associated with the eigenfrequency loci that contain purely acoustic eigenfrequencies in the $n \to 0$ limit. It appears therefore meaningful that a given thermoacoustic mode can be referred to as of acoustic origin or of ITA origin [15]. There is, however, an inconsistency between the definitions given above and the idea of classifying thermoacoustic modes depending on their origin, which we now demonstrate.

For this purpose, we consider a Rijke tube configuration: a straight duct of length 0.5 m with a temperature jump $T_2/T_1 = 4$ across a flame element located in the middle of the tube. Explicit expressions for the dispersion relation of the thermoacoustic eigenvalues can be found in this configuration using network approaches (see [27–29] and §1 in the supplementary material).

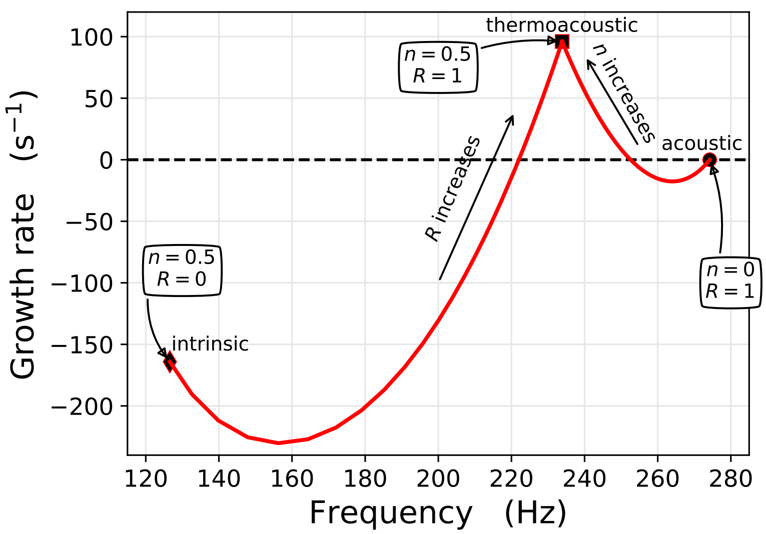

Figure 1: Thermoacoustic mode trajectories while varying the reflection coefficient R or the interaction index n. Depending on which parameter is varied towards zero, the thermoacoustic mode converges to either an acoustic or a pure ITA mode. This illustrates the need for an unambiguous definition of the origin of the thermoacoustic mode origin.

We model the Rijke tube using finite elements, solving the nonlinear eigenvalue problem (1). We use continuation methods – based on high-order adjoint-based eigenvalue sensitivity [30] – to track the evolution of a specific eigenvalue while varying two parameters: the flame interaction index n, and the magnitude of the reflection coefficients $|R|$. The flame time delay is fixed to $\tau = 3.96$ ms. In the fully reflective case, $|R| = 1$, the tube is assumed to be acoustically closed ($R = 1$) in the cold region, and open ($R = -1$) in the hot one. The corresponding non-dimensional impedances (3) are calculated as

$$Z = \frac{1+R}{1-R}. \tag{4}$$

We start by setting $|R| = 1$ (so that the up- and downstream impedances are ∞ and 0, respectively), and $n = 0$. Then, only purely acoustic modes exist, featuring zero growth rate as no damping mechanisms are modeled. An acoustic mode with an angular frequency of 274 Hz is found (see Fig. 1). This value agrees well with that predicted from low-order network models (see supplementary material §1). We then vary the interaction index n and track the eigenvalue evolution. Note that, for small values of the interaction index the flame damps the mode, but for larger values this trend is reversed and the mode becomes unstable. Once we have reached $n = 0.5$, a reasonable value for a flame response, we maintain this value and vary the reflection coefficient magnitudes $|R|$ from 1 to 0. The up- and downstream impedances are calculated according to Eq. (4), with R positive (negative) in the upstream (downstream) region. When $|R| = 0$, the mode is a pure ITA mode. There are analytical expressions available from the literature for pure ITA modes in Rijke tubes (see [1, 3] and supplementary material §1).

These are given by

$$s_{\mathrm{ITA}} \equiv \frac{1}{\tau} \ln \left[\left(\sqrt{\frac{T_2}{T_1}} - 1 \right) n \right] + \frac{(2k+1)\pi}{\tau} \mathrm{i}, \qquad k \in \mathbb{Z}. \tag{5}$$

For the chosen values of n and τ, the resulting intrinsic frequency and growth rate are $f_{\mathrm{ITA}} = 1/(2\tau) \approx 126$ Hz and $\sigma_{\mathrm{ITA}} = -175\ \mathrm{s}^{-1}$, which agree well with the values obtained from the Helmholtz model (see Fig. 1).

2.2. An alternative definition of intrinsic modes

The previous example indicates that there exist thermoacoustic modes that can be arbitrarily associated to either acoustic or pure ITA eigenfrequencies. This depends on whether the parameter responsible for the thermoacoustic coupling is considered to be n or R. With the given definitions of acoustic modes ($n = 0$) and pure intrinsic modes ($R = 0$), it is therefore ambiguous to think of a thermoacoustic mode as of "acoustic" or "ITA" origin. In order to assign to thermoacoustic modes a specific source, the definition of acoustic and intrinsic modes must rely on *one* parameter.

A step in this direction has been done in [14], considering a 1D Rijke tube with an n–τ flame response. Damping, mean flow and entropy-wave effects have been neglected. For this configuration a dispersion relation can be derived, whose zeroes represent the thermoacoustic modes. Using it, it was shown that, when steering n towards zero, any thermoacoustic mode will either reduce to an acoustic mode or move towards an infinitely damped mode, with the same angular frequency as an intrinsic mode, regardless of the boundary conditions. Thus, using only the parameter n it is still possible to identify intrinsic eigenfrequencies, and uniquely associate an origin to each thermoacoustic mode.

These findings are in fact much more general. In the following, we will present a derivation of these results with a method different from that of [14]. Our proof is independent of the dispersion relation and, thus, valid for configurations with mean flow, damping, arbitrary reflection coefficients, and arbitrary expression for the FTF.

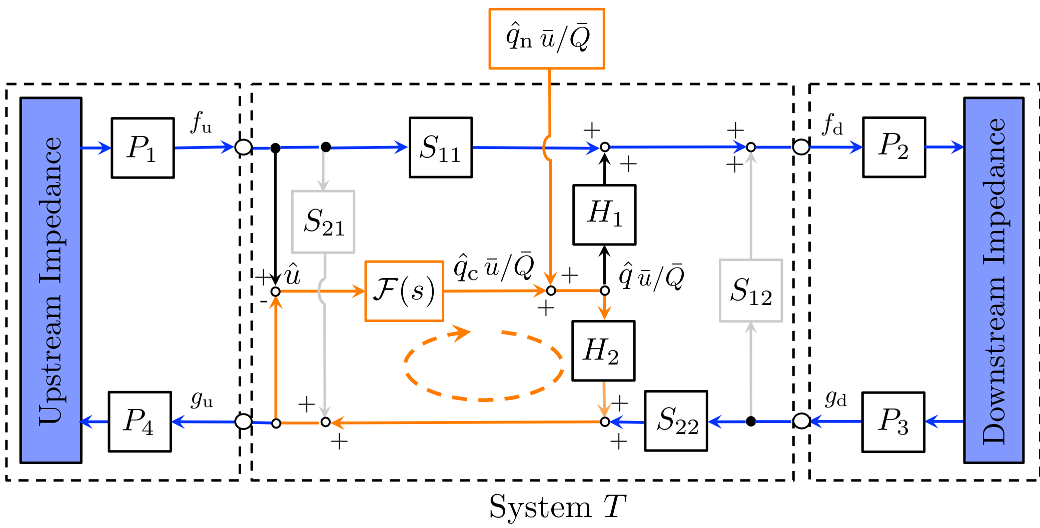

Figure 2: Block-diagram representation of a generic axial combustor. The upstream and downstream impedances can be complex-valued and frequency dependent, so that they can be used to model arbitrarily shaped volumes. The flame is considered compact, so that jump conditions across it can be expressed in terms of a scattering matrix $\mathbf{S}$. The ITA feedback loop is highlighted in orange, and does not involve any interaction with the acoustic boundary conditions.

We consider an arbitrary axial combustor, in which only plane waves propagate, containing an acoustically compact flame. No assumption is made on the actual shape of the setup, presence of a mean flow, or the acoustic boundary conditions. Such a generic configuration can still be represented in block form (Fig. 2), as commonly done in control theory and network model approaches. The propagation blocks, $P_j = e^{-s\tau_j}$, transport the acoustic waves from a location x to $x+\Delta x$. τ_j is a characteristic acoustic propagation time delay [20], proportional to Δx, and generally a function of the mean flow. Damping models add an imaginary term in the exponential of the propagating terms, multiplying s. The jump conditions across the compact flame are contained in the coefficients of the scattering matrix, relating the incident and outgoing acoustic waves:

$$\begin{bmatrix} f_d \\ g_u \end{bmatrix} = \mathbf{S} \begin{bmatrix} f_u \\ g_d \end{bmatrix} + \mathbf{H}\hat{q} = \begin{bmatrix} S_{11} & S_{12} \\ S_{21} & S_{22} \end{bmatrix} \begin{bmatrix} f_u \\ g_d \end{bmatrix} + \begin{bmatrix} H_1 \\ H_2 \end{bmatrix} \hat{q}. \quad (6)$$

The factors H_j account for the scaling between the heat release rate fluctuations and the acoustic waves, and are not frequency dependent (see supplementary material). The coefficients of the scattering matrix, S_{ij}, can in general be function of the frequency, when losses or inertial effects in terms of effective lengths are considered. However, it is standard in the analysis of intrinsic modes in thermoacoustics to assume that they are not, to allow for analytical treatment. The coefficients of $\mathbf{S}$ are derived from jump conditions, which are conservative and show no frequency dependence. Their expression depends on the presence/absence of an area increase/decrease, temperature jump, entropy and/or vorticity waves. The theory presented here is general in this respect, and the definition of the coefficients S_{ij} is kept implicit; an example of their expression is provided in the supplementary material. Lastly, the response of the acoustic configuration upstream and downstream of the flame is modeled by means of arbitrary impedances, which are converted into reflection coefficients R via Eq. (4). These can be complex-valued and/or frequency dependent, and may contain the effects of area variations.

From Fig. 2, considering the balance of the waves at each node, it can be shown that the response of acoustic velocity fluctuations $\hat{u}$ to heat release rate fluctuations $\hat{q}$ is

$$\hat{u} = \frac{(1 - P_1 P_4 R_1)[H_2 + (P_2 P_3 R_2)(H_1 S_{22} - H_2 S_{12})]}{P_1 P_4 R_1 S_{21} + P_2 P_3 R_2 S_{12} + P_1 P_2 P_3 P_4 R_1 R_2 (S_{22} S_{11} - S_{21} S_{12}) - 1} \hat{q}. \quad (7)$$

Assuming that all the components of (7) are analytic functions of the eigenfrequency s, its numerator, $N(s)$, does not have poles. Thus, the *acoustic* eigenfrequencies are those for which the denominator of (7), $D(s)$, vanishes:

$$D(s) := P_1 P_4 R_1 S_{21} + P_2 P_3 R_2 S_{12} + P_1 P_2 P_3 P_4 R_1 R_2 (S_{22} S_{11} - S_{21} S_{12}) - 1 = 0 \quad (8)$$

The heat release rate response, $\hat{q}_c / \overline{Q} = \mathcal{F}(s) \hat{u} / \overline{u}$, is assumed to have no finite poles, for simplicity, although this assumption could be relaxed. This is true for many traditional flame response approximations, including $n - \tau$ models with constant or polynomial coefficients, and more generally for sum of time delay models, which can well fit Flame Transfer and Describing Functions [31, 32].

The ITA loop of the system is highlighted in Fig. 2. It is characterized by the transfer function

$$\hat{q} = \frac{1}{H_2 \mathcal{F}(s) + 1} \hat{q}_n, \quad (9)$$

where $\hat{q}_n$ can be understood as a source of combustion noise [12]. This implies that ITA modes are found when

$$H_2 \mathcal{F}(s) + 1 = 0, \quad (10)$$

which is equivalent to definitions found in the literature [1, 3] for a Rijke tube with anechoic boundary conditions. Coupling the acoustic and flame responses yields the closed-loop transfer function

$$\hat{u} = \frac{N(s)}{D(s) - N(s)\mathcal{F}(s)}\hat{q}_n. \tag{11}$$

The *thermoacoustic* modes are found[1] when $D(s) - N(s)\mathcal{F}(s) = 0$.

One can then track these eigenvalues by slowly varying the gain of the FTF from a finite value towards zero. In the following, we shall assume that $\mathcal{F}(s) = ne^{-s\tau}$, as this permits a direct comparison of our results with those available in the literature, and eases the notation. Two scenarios are possible:

1. $\lim_{n\to 0} |ne^{-s\tau}| \to 0$. Then, for s to be a pole of Eq. (11), the condition $D(s) = 0$ must be satisfied. This coincides with the acoustic modes, as per Eq. (8);
2. $\lim_{n\to 0} |ne^{-s\tau}| \to \mathcal{O}(1)$. This is possible if and only if, asymptotically, $e^{-\sigma\tau} \sim \alpha/n$, with $\alpha \in \mathbb{R}$. This value is not arbitrary, but can be linked to the elements of the scattering matrix and the heat release scaling coefficients H_j (see Appendix A). This implies that

$$\sigma \sim \frac{1}{\tau}\log(n/\alpha) \qquad \text{as } n \to 0, \tag{12}$$

   and that $\lim_{n\to 0} ne^{-(\sigma+\mathrm{i}\omega)\tau} \propto e^{-\mathrm{i}\omega\tau}$. In other words, the infinite growth rate of the time-delayed terms is balanced by the vanishing flame strength when $n \to 0$. We now want to find those values of s that are poles

[1] This assumes that no zero–pole cancellations, which are nonetheless extremely rare, occurs; otherwise, some extra modes are identified.

of (11) in this limit. It can be shown (see Appendix A) that the angular frequencies of these infinitely damped modes are identical to those of ITA modes (Eq. (5)).

This proves that, in the $n \to 0$ limit, thermoacoustic modes are split into two distinct sets. One of them is equivalent to the set of acoustic modes, the other is connected to the ITA modes (with infinite damping), regardless of the boundary conditions.

We remark that the intrinsic loop highlighted in Fig. 2 and defined in Eq. (10) exists in an isolated fashion only when no area variations are present in the volumes upstream/downstream of the flame. Otherwise, even when purely anechoic boundary conditions are imposed, reflection of acoustic waves will occur due to the area changes. This modifies the anechoic intrinsic loop and the consequent definition of pure intrinsic modes, as discussed in [7]. This is, however, unimportant in the current analysis because only the limit $n \to 0$ is considered. The amplitude of the ITA generated waves that propagate away from the flame vanish in this limit because they are infinitely damped, regardless of the presence of area variations. As a consequence of this, the definition of intrinsic modes for vanishing n depends only on the values of the scattering matrix and flame scaling coefficients, as shown in Appendix A.

Using a single parameter to define both acoustic and ITA frequencies allows for unambiguously associating each thermoacoustic mode with a specific origin. This is not possible when different parameters are used to define ITA and acoustic modes. Here, the chosen parameter is the flame gain (as it retains the natural definition of acoustic modes), but the reflection coefficient could be chosen equivalently (which would lead to a different, but still unique, classification of the eigenvalues).

Furthermore, the results of this section have an important consequence for practical applications and the numerical calculation of thermoacoustic modes. Commonly, thermoacoustic modes are found by initializing Helmholtz solvers with the purely acoustic frequencies (found when $n = 0$) and then by gradually increasing the value of n and track the evolution of the eigenvalues [33]. However, this method fails in identifying all thermoacoustic modes, as some modes are of ITA origin. Using the results of this proof, we have a new set of guesses that can be used to identify the remaining thermoacoustic modes: starting from a small but non-zero value of the interaction index, thermoacoustic modes of intrinsic origin are approximately given by Eq. (A.5). No other modes can be found because, when $n \to 0$, all modes *must* belong to one of these two sets. Once located in this limit, all thermoacoustic eigenvalues can be tracked to the desired value of n using continuation methods. Thus, with this strategy the space that needs to be explored is limited to that in the vicinity of the theoretically estimated solutions. This leads to a gain in both the numerical time needed to locate the thermoacoustic modes, and in the confidence that all modes (in a given frequency range) have been identified. This will be demonstrated in §4.

2.2.1. The annular combustor case

In this section we qualitatively discuss how the results of §2.2 can be extended to annular and can-annular thermoacoustic configurations. In particular, we will consider systems featuring a discrete rotational symmetry. Such systems are generally modeled with two acoustic volumes connected by

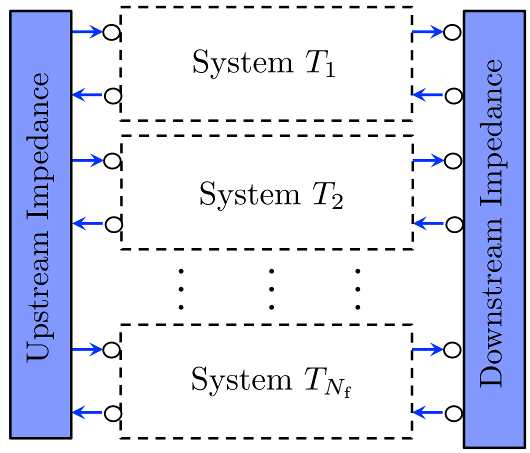

Figure 3: Block-diagram representation of an annular combustor with discrete rotational symmetry and N_f flames. The flames are located in ducts that connect upstream and downstream acoustic cavities (annular plenum and annular combustion chamber).

N_f ducts, in which identical flames are located (see Fig. 3). The acoustic boundary conditions couple the responses of the various ducts, in which the acoustic field is assumed to be one dimensional, and can be modeled with impedance matrices [34, 35]. These contain the acoustic response in all the ducts when the acoustic field in a given duct is excited. Given the rotational symmetry of the system, these matrices are circulant, which has direct connections with a possible Bloch representation of the dynamics [36–38].

In the limit $n \to 0$, the same results of the previous section must hold for each duct. In this limit, there is no physical mechanism that couples the N_f intrinsic loops. Since the flames in the various ducts are identical, so are all intrinsic loops, which are still governed by the dispersion relation (10). This results in N_f identical intrinsic eigenfrequencies, infinitely damped, and with the same frequency of pure ITA modes. This discussion is kept qualitative because, given the matrix formulation needed to represent annular systems with discrete symmetries, a closed-form formulation of analytical results is impractical.

These intrinsic loops can be thought of as a set of identical, decoupled oscillators. A weak coupling between them is achieved by either considering small but non-zero up- and downstream reflection coefficients when the flame interaction index is finite, or a small but non-zero flame interaction index when the reflection coefficients are finite. In both cases, the dynamics of ITA modes is governed by weakly coupled oscillators. When identical oscillators are weakly coupled, the eigenvalues of the weakly coupled system form clusters of closely spaced eigenvalues [39]. This is the case, for example, in can-annular systems, in which the acoustic coupling between the various cans is weak, and clustering of thermoacoustic modes can be observed [40]. The same holds true for modes of ITA origin in annular systems. This has been first observed numerically in [41], where clusters of modes with eigenfrequencies close to those of ITA modes were found.

3. Interaction of acoustic and intrinsic modes with exceptional points

In the previous section, we have discussed how the origin of thermoacoustic modes can be assessed using only the interaction index n of the flame. There remain however some points in the spectrum of thermoacoustic systems that elude this classification. These points are known as exceptional points (EPs). EPs are a particular type of degenerate, defective eigenvalues, with the additional property of being singularities in the parameter space [42]. EPs have recently been identified in the spectrum of a Rijke tube-like thermoacoustic system using an explicitly known dispersion relation [19]. Here, we show how EPs of any thermoacoustic systems can be identified numerically without using the dispersion relation, but the self-orthogonality property of the eigenfunctions at EPs.

3.1. Self-orthogonality

The eigenvalue sensitivity of thermoacoustic modes w.r.t. a parameter ξ is given by [43, 44]:

$$\frac{\partial s_j}{\partial \xi} = -\frac{\left\langle \hat{\boldsymbol{p}}_j^\dagger \middle| \frac{\partial \mathbf{L}}{\partial \xi} \hat{\boldsymbol{p}}_j \right\rangle}{\left\langle \hat{\boldsymbol{p}}_j^\dagger \middle| \frac{\partial \mathbf{L}}{\partial s} \hat{\boldsymbol{p}}_j \right\rangle}\Bigg|_{s=s_j}, \tag{13}$$

where the adjoint eigenvectors have been denoted with the superscript †, and the matrix $\mathbf{L}$ contains the discretization of the thermoacoustic eigenvalue problem (1). Equation (13) is valid whenever the denominator is non-zero. This is always guaranteed to be the case for non-defective eigenvalues (even if they are degenerate), but it is zero for defective eigenvalues [45]. In fact, the derivation of equation (13) assumes that a bi-orthonormal set of direct/adjoint eigenfunctions can be chosen [46]:

$$\left\langle \hat{\boldsymbol{p}}_i^\dagger \middle| \frac{\partial \mathbf{L}}{\partial s} \hat{\boldsymbol{p}}_j \right\rangle = \delta_{i,j}. \tag{14}$$

This breaks down at defective points, because the basis of the eigenvectors is incomplete. In particular, it is possible to show that, for defective eigenvalues, the direct and corresponding adjoint eigenvectors satisfy [47]

$$\left\langle \hat{\boldsymbol{p}}_{\text{def}}^\dagger \middle| \frac{\partial \mathbf{L}}{\partial s} \hat{\boldsymbol{p}}_{\text{def}} \right\rangle = 0. \tag{15}$$

This property is known as self-orthogonality. At EPs, it manifests itself in infinite eigenvalue sensitivity. We reference to the supplementary material §2 for remarks on numerical aspects of self-orthogonality.

3.1.1. General method for the identification of exceptional points

We exploit the infinite eigenvalue sensitivity at EPs to devise a general strategy for their identification in thermoacoustic systems. At EPs, we have

$$\lim_{\xi \to \xi_{\mathrm{EP}}} \left| \frac{\partial s}{\partial \xi} \right|^{-1} = 0 \tag{16}$$

Thus, the identification of EPs is reduced to a root-finding problem, which can be straightforwardly solved numerically with iterative methods. Note that, every time the parameter ξ is updated in the iterative scheme, a new eigenvalue problem needs to be solved, and the sensitivity can then be calculated using Eq. (13). Furthermore, since the eigenvalues of thermoacoustic problems are generally complex-valued, also the value of the parameter ξ at which the EP is found using this strategy can be complex-valued. These complex-valued parameters may or may not be physically realizable: an EP found in a Rijke tube having a complex-valued length would not be realizable, but one found for a complex-valued impedance would. In order to identify EPs for real-valued parameters, we need to extend the parameter space under consideration to two independent parameters [42]. The identification of EPs in the real-valued parameter space reads

$$\lim_{\substack{\xi_1 \to \xi_{1,\mathrm{EP}} \\ \xi_2 \to \xi_{2,\mathrm{EP}}}} \left| \frac{\partial s}{\partial \xi_i} \right|^{-1} = 0 \qquad \text{for } i = 1 \text{ or } 2, \tag{17}$$

which can be solved using standard multi-parameter root finding algorithms.

Despite their peculiar nature, EPs are not rare, and have been observed in a large variety of physical systems [48]. In thermoacoustics, they have been first discussed only recently [19]. In the latter study, they have been identified making use of the dispersion relation for the eigenvalues, which is available only for simple networks. The method outlined in this study is more general because it does not rely on the explicit knowledge of the dispersion relation, which is typically not available, for instance, when using Helmholtz solvers. The method has been tested on several configurations. For all tested cases, identifying real-valued EPs was possible, as discussed in §4.

Lastly, we highlight that there appears to be evidence in the literature that the effects of EPs in the spectra of thermoacoustic systems, even if not investigated directly, have already been observed. In [49], eigenvalues having infinite sensitivity have been identified analytically, in a Rijke tube-like system. They have however imprecisely been linked to arbitrary degenerate states rather than to EPs. Large eigenvalue sensitivities were also observed in [50], together with the phenomenon of mode veering. Mode veering is a manifestation of avoided crossing of two eigenvalues. This always occurs when the thermoacoustic system parameters are close to a degenerate point, at which the eigenvalue trajectories intersect. The behavior of the eigenvalue trajectories tells whether the degeneracy is defective or not. For a degenerate eigenvalue with multiplicity 2, if the trajectories approach each other from nearly opposite direction and then veer by 90° (as is the case in [50]), then there is an EP close in parameter space, at which the eigenvalue sensitivity is infinite [42]. On the other hand, if the trajectories veer at different angles, then the veering is due to a degenerate, non-defective point, and the eigenvalue sensitivity remains finite. The existence of EPs is evident also in [26, 51], where regions of high sensitivity exhibiting mode veering have been identified, and their universality in connection to non-dimensional groups has been demonstrated. Regarding annular combustors, the presence of EPs can be inferred from the eigenvalue trajectories shown in [52, Fig. 8] and [53, Fig. 6], constructed while varying n and τ. This example will be further discussed in §4.2.

3.2. The effect of exceptional points on thermoacoustic eigenvalue trajectories

We shall now return to the Rijke tube example of §2.1. Using the numerical method outlined in the previous section, with $\xi_1 = n$ and $\xi_2 = \tau$, an EP is identified in this configuration for $n_{\mathrm{EP}} = 0.075$ and $\tau_{\mathrm{EP}} = 4.66$ ms, having a frequency close to that of the acoustic mode of Fig. 1 and a negative growth rate. Starting from the EP, we vary the flame gain n in the range [0,0.5] and the reflection coefficient $|R|$ in the range [0,1.3]. The resulting eigenvalue trajectories are shown in Fig. 4.

One of the two trajectories obtained while varying n starts (for $n = 0$) at the acoustic eigenvalue (on the neutral line); the other comes instead from a very negative growth rate. On the contrary, the two trajectories obtained while varying R start (for $R = 0$) from pure ITA modes, whose values estimated from Eq. (5) are reported with red circular markers in Fig. 4. The trajectories meet at the exceptional value, and turn by 90° across it. Furthermore, because no discontinuities in the parameters are present in the modeled system, the eigenvalue trajectories must be continuous. In the vicinity of the exceptional point, this means that the trajectories must strongly veer, to avoid a crossing. This explains the behavior of the eigenvalue trajectory shown in Fig. 1: increasing n, the eigenvalue trajectory is first attracted towards the EP, which has a negative growth rate. However, since crossing is prohibited, the trajectory must strongly veer, which leads to a sudden change in the trend of the eigenvalue sensitivity and eventually to the existence of

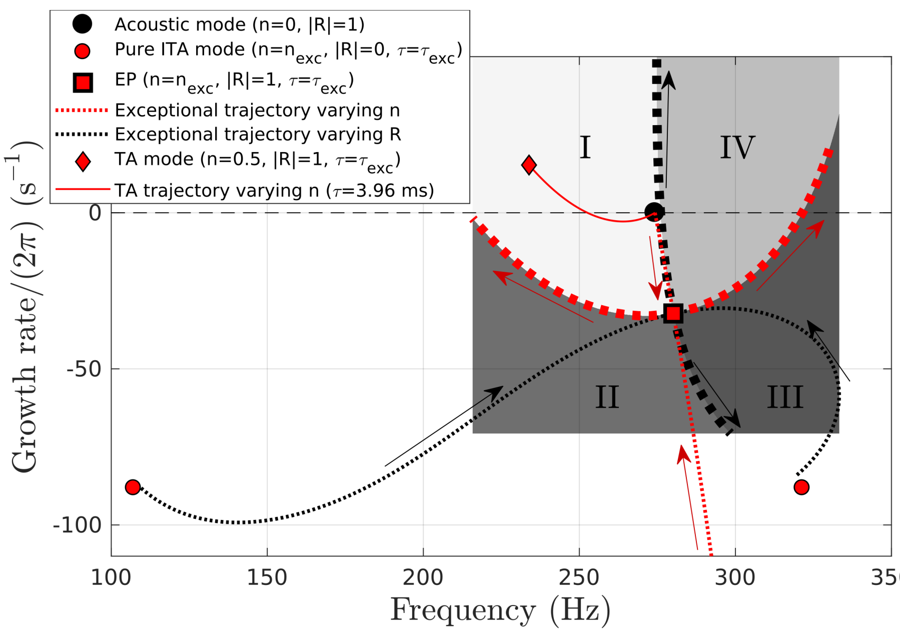

Figure 4: Behaviour of the eigenvalue trajectories obtained while varying the flame interaction index and reflection coefficients across an EP. The arrows indicate the direction that the trajectories follow when the parameters are increased. The acoustic solution is marked with a black circle, and the pure ITA modes for $\tau = \tau_{\mathrm{EP}}$ with red circles. Because trajectories cannot intersect in the vicinity of an EP, four regions, labelled I to IV, corresponding to different behaviors in the limits $n \to 0$ and $R \to 0$ are identified. The thermoacoustic mode and the eigenvalue trajectory of Fig. 1 lie in region I.

an unstable mode. This is true even though the identified EP has a negative growth rate. Rather than the EP per se, it is its interaction with the eigenvalue trajectories which is relevant: identifying the parameters at which EPs are found gives information about when strong changes in the eigenvalues sensitivities are expected. As demonstrated in Fig. 4, this sudden change in sensitivity can lead to thermoacoustic instabilities.

The fact that eigenvalue trajectories cannot cross in the vicinity of an

EP leads to a classification of the eigenvalue space in its vicinity. Consider the exceptional trajectories for n highlighted with thick red lines in Fig. 4: the acoustic mode is contained in the portion of the plane above this line. Because eigenvalue trajectories cannot intersect, thermoacoustic modes that start above this line must converge to the acoustic mode when $n \to 0$. On the other hand, modes that start below this line cannot converge to an acoustic mode when $n \to 0$, and will be pushed towards $\sigma \to -\infty$. Similarly, the exceptional trajectories for R highlighted with thick black lines in Fig. 4 delimit the region of convergence towards two separate pure ITA modes when $R \to 0$: on the left, eigenvalues must be attracted towards the ITA mode with frequency $1/(2\tau)$; on the right, towards the ITA mode with frequency $3/(2\tau)$. Thus, four regions exist (I-IV in Fig. 4) in which the behavior of the eigenvalues in the limits $n \to 0$ and $R \to 0$ differs. For example in region I (top–left), eigenvalues must be attracted towards an acoustic solution when $n \to 0$ and to the ITA solution with frequency $1/(2\tau)$ when $R \to 0$. Similar arguments hold for the remaining regions. The thermoacoustic mode shown in Fig. 1 lies in region I in Fig. 4, which is consistent with the seemingly ambiguous $n \to 0$ and $R \to 0$ limits.

In summary, the "basins of attraction" of acoustic and pure ITA modes are determined by the parameter chosen to describe the thermoacoustic coupling. Because the exceptional trajectories for varying n and R are different, the resulting basins differ too. This explains why a classification of the thermoacoustic modes using two separate parameters can be ambiguous. These findings on the identification of EPs and the behavior of eigenvalue trajectories in their vicinity are general, and will be demonstrated on more complex geometries in the last part of the study.

4. Numerical examples

In this section we demonstrate with two examples (an axial and an annular configurations) the theoretical findings of this study. Both cases are solved using the freely available 3D FEM code PyHoltz[2], dedicated to (thermo)acoustic eigenvalue problems.

4.1. BRS combustor

As an axial configuration, we focus on the so-called BRS combustor [54]. Thermoacoustic oscillations with a frequency which is not close to any acoustic mode have been experimentally observed in this combustor [9], and have been related to the effect of ITA modes in the literature [13]. The modeled combustor is shown in Fig. 7 (see the aforementioned references for an exhaustive geometrical description of the combustor).

We assume that the inlet/outlet are respectively acoustically closed and open, and that a sudden temperature jump, $T_2/T_1 = 5.46$, occurs across the flame. Starting from the purely acoustic scenario ($n = 0$, fully reflective boundaries), we identify several acoustic modes having zero growth rate. The lowest two frequencies correspond to a Helmholtz mode with $f_H = 54$ Hz and a quarter-wave like mode, with a frequency of $f_{1/4} = 589$ Hz, and are shown in Fig. 5.

We then set the interaction index to the small value $n = 0.001$ and the time delay (arbitrarily) to $\tau = 6.88$ ms. The eigenvalues of this thermoacous-

[2]Freely available at https://bitbucket.org/pyholtzdevelopers/public

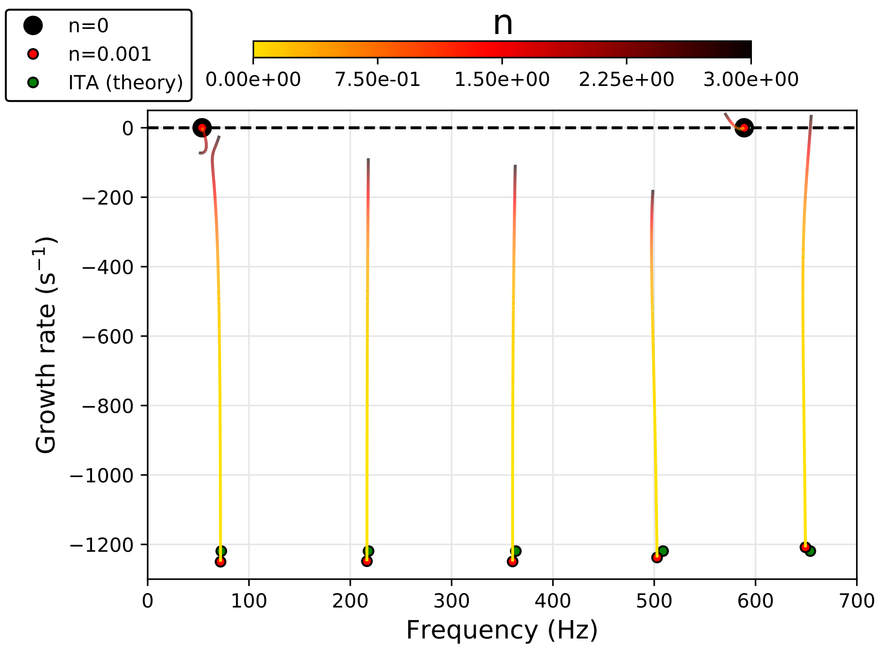

Figure 5: Location of the acoustic (black circles) and thermoacoustic (red circles) eigenvalues when $n = 0$ and $n = 0.001$, respectively. The theoretical guesses for the locations of the thermoacoustic modes of ITA origin are indicated with green markers. The lines track the eigenvalue trajectories for $n \in [0.001, 3]$.

tic system are shown in Fig. 5 with red markers; because of the weak effect of the flame, the eigenvalues of acoustic origin are almost unaffected. However, a new set of modes, having ITA origin, is found. These modes have been identified using as guesses the expression (A.5), with $\beta^{-1} = (\theta^2 - 1)/(A_r\theta + 1)$, obtained from (A.3) when a temperature jump ($\theta = \sqrt{T_2/T_1}$) and an area jump ($A_r = A_2/A_1 = 7.95$) are found across the flame, and mean flow is neglected. The theoretical guesses are marked in Fig. 5 with green circles, and are used to initialize the search of thermoacoustic eigenvalues via Newton's method. The converged thermoacoustic eigenvalues for $n = 0.001$ are marked with red circles, and agree well with the theoretical predictions. The configuration at hand has an area jump upstream of the flame, which affects the definition of pure ITA modes in the anechoic limit [7]. However, this has no effect on the definition of the ITA modes originating in the limit $n \to 0$.

Using these initial guesses, we can then track the evolution of *all* thermoacoustic eigenvalues in the region of interest while increasing the value of the interaction index to any desired value. These trajectories are shown with lines in Fig. 5: the growth rates of thermoacoustic modes of ITA origin are far more sensitive to changes in n than the growth rate of the modes of acoustic origin. For large values of n, the modes of ITA origin can become unstable and feature the largest growth rates. Also, mode veering between an eigenvalue of acoustic origin and one of ITA origin is visible at a frequency of about 60 Hz.

This mode veering is relevant for the experimental observations of [9], where oscillations with a frequency of 100 Hz were observed, and have been associated to an ITA mode instability [4]. Therefore, we shall focus the attention around the low-frequency Helmholtz mode only. To understand the influence of the flame response on the spectrum, we vary $n \in [0, 3]$ and $\tau \in [0, 0.016]$. The maximum τ is chosen to be $< 1/f_H$, to avoid that eigenvalue trajectories intersect in the vicinity of the acoustic solution. The resulting stability map is shown in Fig. 6; as commonly observed, depending on the particular choice of both n and τ, the resulting thermoacoustic mode can be stable or unstable. In the vicinity of the acoustic solution the eigenvalue sensitivity with respect to changes in the interaction index is nonlinear: a small increase in n from zero first stabilizes the pole, but the trajectory

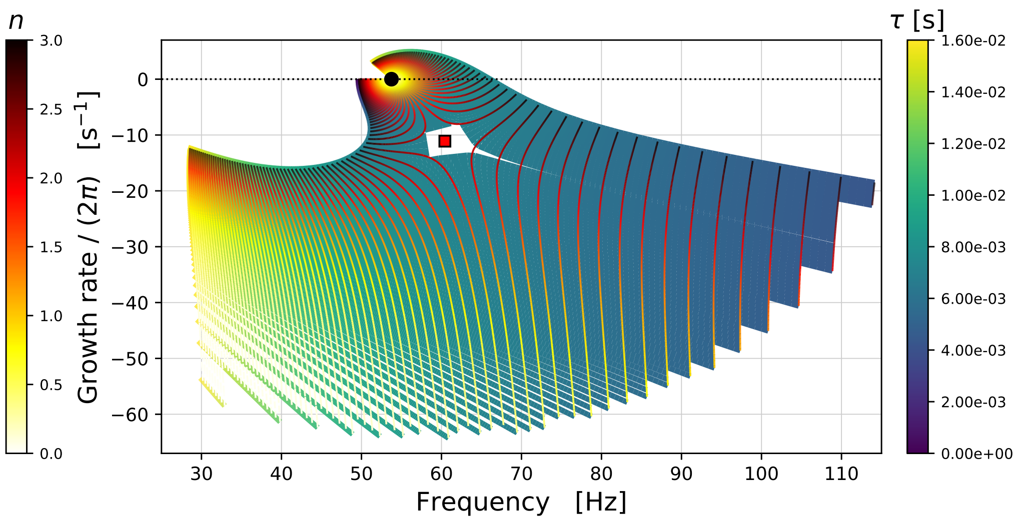

Figure 6: Trajectories of the lowest frequency eigenvalue of the BRS combustor when varying the parameters of the flame model. The trajectories with constant n and constant τ are highlighted with different colormaps. The acoustic solution ($f = 53.75$ Hz) is highlighted with a black circle. In the region which is avoided by the eigenvalues, there exists an EP ($n_{\mathrm{EP}} = 2.181$, $\tau_{\mathrm{EP}} = 6.96$ ms), indicated in red. The local behavior of the trajectories in this region is shown in Fig. 8a.

strongly veers and the mode can become unstable for larger values of n, as was observed in Fig. 1. Because of their veering, which can be observed for both the n- and τ-isolines, the eigenvalue trajectories avoid a region in the complex-frequency space, as discussed in [26]. The presence of this avoided region is one of the characteristics of EPs. Its existence can be confirmed using the procedure outlined in §3.1: starting from an educated guess based on Fig. 6, a root of Eq. (17) is found while varying n and τ. This root identifies an EP (see Fig. 8). Its modeshape is reported in Fig. 7, together with that of the purely acoustic Helmholtz mode (plenum dominant) and of the mode of ITA origin in the $n \to 0$ limit (flame region dominant). These are the two modes that coalesce to create the EP, whose modeshape has clearly inherited features from both of them.

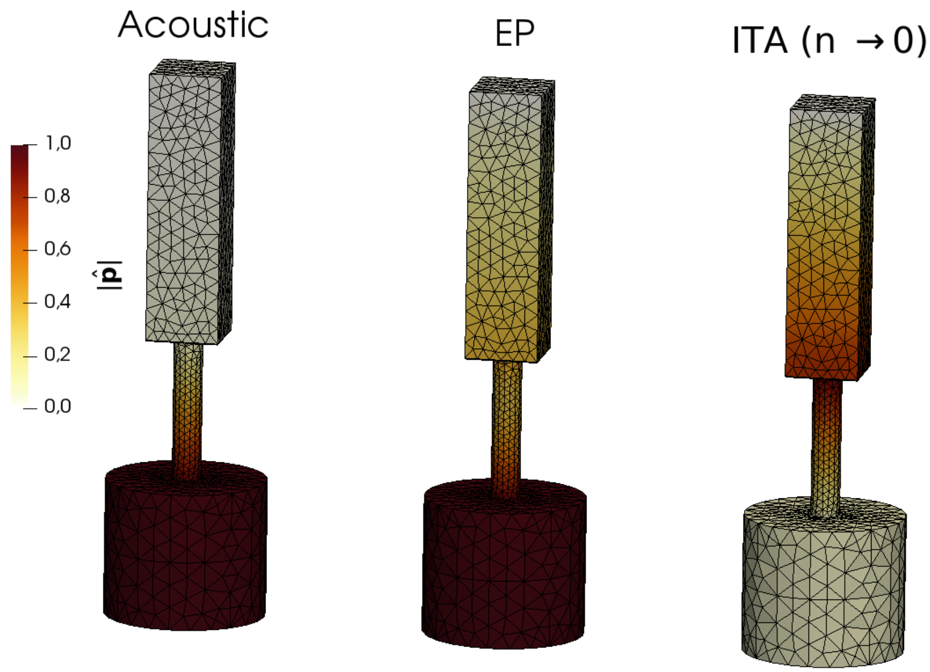

Figure 7: Geometry of the BRS combustor and pressure modeshapes of the low-frequency acoustic (left), ITA origin (right) and exceptional (middle) modes.

The trajectories of the eigenvalues around the EP are shown in Fig. 8. At the EP, two eigenvalues, one of acoustic and one of intrinsic origin, coalesce. Due to the high sensitivity of the eigenvalues in the vicinity of the EP, a small parameter range is considered. When one parameter (n or τ) is fixed at the exceptional value and the other is varied, the trajectories collide at the EP, and branch off at angles of 90° (Fig. 8a). The further the parameter values are from those of the EP, the less intense is the veering. Figures 8b and 8c show the frequency and growth rate surfaces as functions of n and τ close to the EP. Because real and imaginary part of the eigenvalue surfaces are

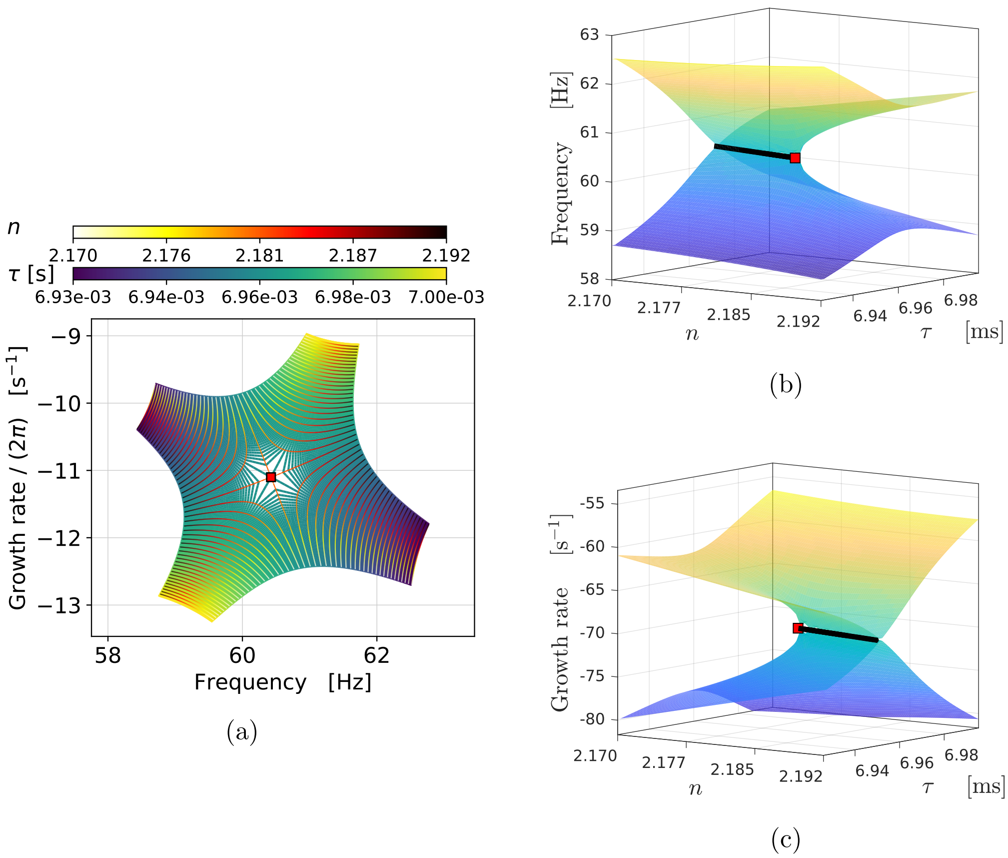

Figure 8: (a): Trajectories of the eigenvalues in the vicinity of the EP. At the EP the trajectories cross forming right angles. (b)-(c): Frequency and growth rate surfaces as functions of n and τ close to the EP. The Riemann cuts of the surfaces are highlighted with black lines, the EP in red.

plotted separately, each surface self-intersects, forming Riemann cuts [18]. The number of eigenvalues found for an arbitrary pair of values (n, τ) close to the EP is equal to the number of intersections of vertical lines passing through (n, τ) with the complex-valued surface. This is always equal to 2 in Figs. 8b and 8c, except at the EP at which it is equal to 1, indicating eigenvalue crossing.

Our analysis of the BRS system is consistent with the theoretical discussion that thermoacoustic modes can uniquely be classified as of acoustic or ITA origin in the limit $n \to 0$, regardless of the boundary conditions and presence of area variations upstream of the flame. An EP exists in the spectra of this combustor for specific values of n and τ, at which two eigenvalues (one of acoustic and one of intrinsic origin) coalesce. Even if the system is not operated at EP conditions, being sufficiently close to it in parameter space results in strong mode veering. This can explain why the unstable frequency observed experimentally in [9] significantly differs from all the acoustic eigenfrequencies of the system, although the unstable mode may still be of acoustic origin.

4.2. Annular configuration

As for an annular configuration, we consider the Helmholtz model of a generic geometry formed by plenum and chamber volumes connected by a given number of ducts (see Fig. 10). These configurations can also be analyzed using network models, as discussed in [35, 55–57]. We investigate the $N_f = 4$ burners setup presented in [52] because (i) the configuration has closely spaced acoustic eigenvalues, and (ii) different regimes (uncoupled, weakly coupled, and strongly coupled) have been identified in [52], which are revisited here. This will show that the occurrence of these different regimes can be explained with the existence of EPs.

The geometrical and thermodynamical parameters are taken from [56], with the difference that a smaller temperature jump has been considered, $T_2/T_1 = 1.5$, in order to have closely spaced acoustic eigenvalues when $n = 0$, as in [52]. The two acoustic eigenvalues with the lowest frequencies are reported with black circles in Fig. 9. The two modes are plenum- and chamber-dominant, respectively, with azimuthal order $m = 1$, therefore degenerate. Their modeshapes[3] are reported in Fig. 10, and the frequencies are close to the frequencies of the plenum/chamber, $f_i = c_i/(\pi D_i)$, where D_i are the diameters of the volumes. The deviation from these values is due to the cross-talking of the plenum-chamber volumes via the connecting ducts.

To investigate the effect of the flame response on the eigenvalues, we vary $n \in [0, 2]$ and $\tau \in [0, 0.015]$ s. The maximum time delay value is chosen to be $1/f_{\text{chamber}}$ so that eigenvalue trajectories looping around the acoustic eigenvalues will not cross each other [26, 58]. We track the eigenvalues using continuation methods and show the eigenvalue trajectories in Fig. 9. In the range of parameters studied, we identify three topologically different groups of eigenvalue trajectories:

I. when $n < 1.17$, varying τ results in looping the thermoacoustic eigenvalues that originate from the plenum and chamber acoustic modes around these solutions. This corresponds to the "weakly coupled" regime discussed in [56], in which it is appropriate to associate each thermoacoustic mode to an acoustic mode.

II. when $1.17 < n < 1.44$, the trajectories do not follow closed loops anymore. The thermoacoustic eigenvalue that starts close to the plenum acoustic mode is shifted towards a value close to that of the chamber

[3] Because these solutions are degenerate with geometric multiplicity 2, they each have 2 linearly independent modeshapes. Only one of them is shown in Fig. 10.

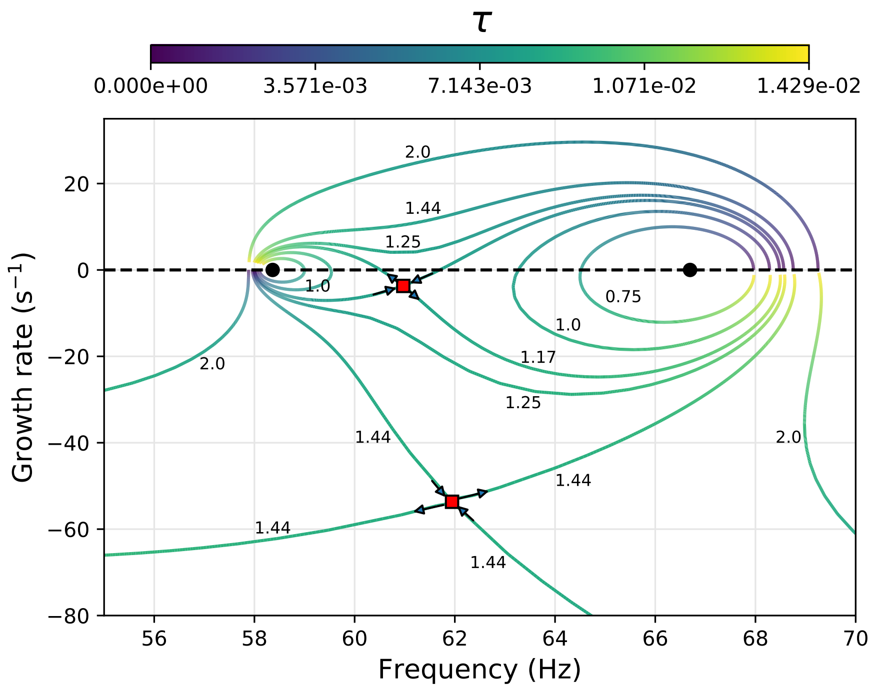

Figure 9: Eigenvalue trajectories of the annular configuration for constant n (isoline values) when τ is varied. The system has two closely spaced purely acoustic eigenvalues (black dots). Two exceptional points (red squares) are identified: one due to the interaction between two modes of acoustic origin, close to the real axis, and one due to the interaction between acoustic and intrinsic modes. The values of n at which EPs are located determine topological changes in the eigenvalue trajectories.

acoustic mode, and vice versa. In other words, the nature of these thermoacoustic modes strongly varies depending on the value of τ considered. For intermediate values of τ, the modes have frequencies which lie between those of the two acoustic modes, and their modeshapes are not anymore dominant in only the plenum or chamber, but instead in both cavities (see Fig. 10). For this reason, in this regime, which corresponds to the "strongly coupled" regime of [56], it would be inappropriate to

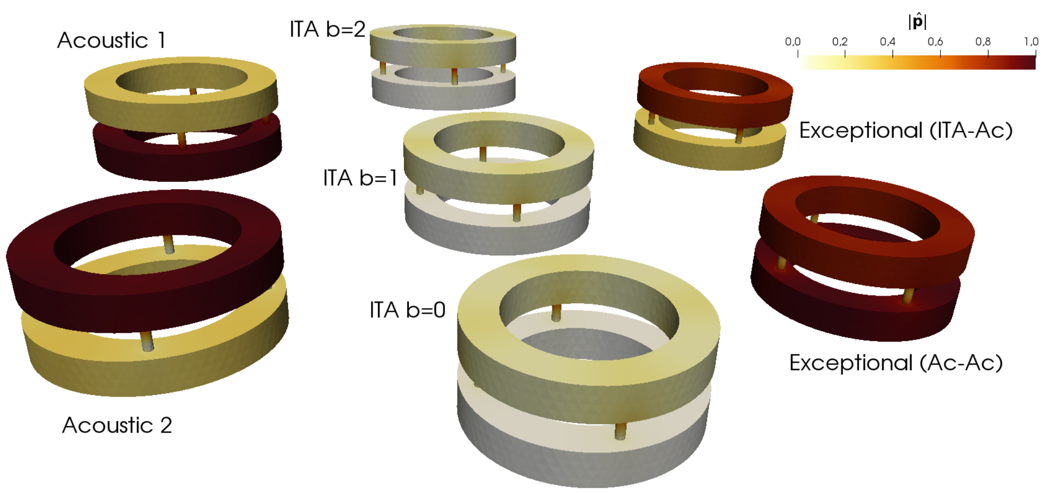

Figure 10: Absolute value of the pressure of various modes found in the annular combustor configuration. Left column: plenum and chamber dominant acoustic modes (see Fig. 9). Middle column: cluster of ITA modes found in the limit $n \to 0$ (see Fig. 11); the modeshapes are identical and dominant in the flame region, as expected for ITA modes. Right column: modeshapes of the two identified exceptional points (see Fig. 9). One is due to the interaction between two modes of acoustic origin, the other between a mode of acoustic origin and one of ITA origin.

perform a single-mode (degenerate) Galerkin expansion. A two-mode Galerkin expansion that accounts for both the plenum- and chamber dominant modes should yield a good approximation, as hinted by the modeshapes shown in both Figs. 7 and 10.

III. Another topological change in the eigenvalue trajectories is observed when $n > 1.44$. The eigenvalues that start close to the chamber acoustic mode are shifted towards plenum-dominant solutions when τ increases, as in the previous regime. The same is, however, not anymore true for the other eigenvalue. The mode that starts close to the plenum-dominant solution is pushed away from any known acoustic solution, and a trajectory that starts from a solution that is not related to any known acoustic mode (on the right of Fig. 9) ends with a frequency close to the chamber-dominant acoustic mode. In this regime, which has not been discussed before, also a two-mode Galerkin expansion based on the acoustic modes cannot yield a good approximation of the original system, because the thermoacoustic modes can be significantly different from the acoustic ones.

From the topological structure of the various eigenvalue trajectories, it is possible to infer that EPs must exist for specific pairs of n and τ. These EPs in fact discriminate between the three regimes just discussed. Starting from educated guesses based on shape of the eigenvalue trajectories, and using the numerical procedure outlined in §3.1, we identify two EPs in the parameter region investigated. One is found for $n_{\mathrm{EP},aa} = 1.17$ and $\tau_{\mathrm{EP},aa} = 8.19$ ms, and discriminates between the aforementioned regimes I and II. The other is found for $n_{\mathrm{EP},ai} = 1.44$ and $\tau_{\mathrm{EP},ai} = 8.91$ ms, and discriminates between regimes II and III.

The first EP is labelled with the subscript $_{\mathrm{aa}}$ because it results from the collision of two modes of acoustic origin. In [19] only EPs that arise from the interaction of a mode of acoustic origin and one of ITA origin were discussed. EPs arising from two acoustic eigenvalues are already known from the discussions of EPs in acoustic systems, and have a relevance, e.g., in optimizing the performance of Helmholtz dampers [18, 59]. However, in the current example the coalescence of two eigenvalues of acoustic origin at the EP is driven by the flame response parameters. Such EPs were not discussed in the literature before. The acoustic–acoustic nature of this EP is also visible in its modeshape, shown in Fig. 10: in contrast to the acoustic modes – purely plenum- or chamber dominant – this modeshape has the same magnitude in both cavities, suggesting that a single-mode Galerkin expansion (that preserves only the plenum's or chamber's structure) would not be a suitable approximation in its vicinity.

The other EP is labelled with the subscript $_{\mathrm{ai}}$ because it originates from the interaction between modes of acoustic and ITA origin. Its behavior is analogous to that discussed in §4.1 and [19], as is more evident from Fig. 11: starting from $n_{\mathrm{EP},ai}$ and decreasing the value of n towards zero, two eigenvalues stem from this EP: one converges to an acoustic solution (that of the chamber), the other tends towards an ITA mode. Also, because of the discrete rotational symmetry of the annular configuration under investigation, each eigenvalue shown in Fig. 9 is degenerate with algebraic and geometric multiplicity 2. As both EPs identified for this configuration are found when 2 eigenvalues (each having algebraic multiplicity 2) coalesce, the EPs have algebraic multiplicity 4, but are defective in that only two linearly independent modeshapes exist, i.e. they have geometric multiplicity 2. Only one of these modeshapes is shown in Fig. 10, the other is phase-inverted, as for degenerate (thermo)acoustic modes.

Lastly, we verify that, for annular configurations, in the limit $n \to 0$ the N_f modes of ITA origin are almost decoupled, as discussed in §2.2.1. Thus, a cluster of $N_f = 4$ eigenvalues of ITA origin is expected to be found in the vicinity of the value predicted by Eq. (A.5). Starting from this theoretical guess, a Newton method is employed to identify the close eigenvalues. Given the fact that the modes cluster, however, it is difficult to identify all

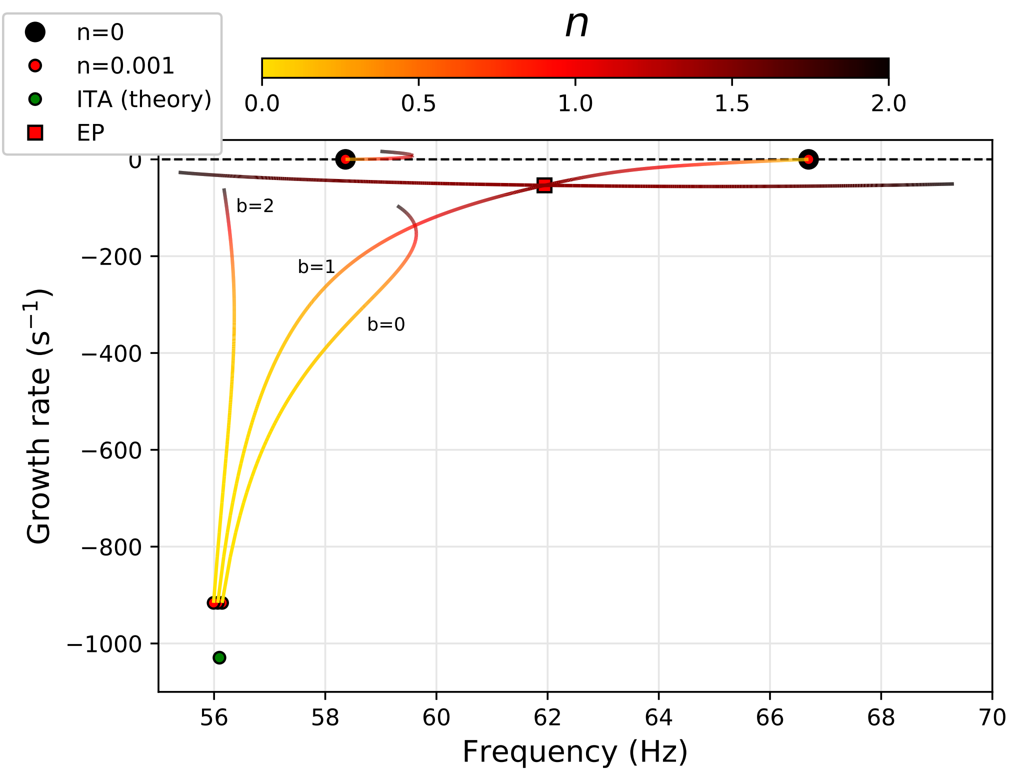

Figure 11: Modes of ITA origin found in the annular setup when $n \to 0$. The cluster of ITA modes estimated using equation (A.5) for $n = 0.001$ is shown in green. Four thermoacoustic eigenvalues (one for each burner, and two are degenerate due to the symmetries of the annular configuration) are found in its vicinity. The lines track all the eigenvalues for $n \in [0.001, 2]$: two modes of ITA and acoustic origin coalesce at $n_{\mathrm{EP},ai}$.

the modes, as the iterative algorithm tends to converge to the same solution. Bloch-wave theory comes to aid [37]. By using this formalism, the clustered modes are naturally split across the various Bloch-wave numbers $b = 0, 1, \ldots N_f - 1$. In the $n \to 0$ limit, a mode of ITA origin is found for each Bloch-wave number for the configuration at hand when $n = 0.001$, as shown in Fig. 11. Because of the mirror symmetry of the system, the modes found for $b = 1$ and $b = 3$ are degenerate for any value of n. In general, for a system with an even number N_f of burners, the cluster of eigenvalues found in the $n \to 0$ limit will be formed by $N_f/2+1$ distinct eigenvalues, of which $N_f/2-1$ are degenerate with multiplicity 2. We can then track these solutions of ITA origin by increasing n towards any desired finite value. The eigenvalue trajectories are shown in Fig. 11. Because we have fixed the time delay to $\tau_{\mathrm{EP},ai}$, we identify again the EP of acoustic–intrinsic nature. Notably, only the mode of ITA origin with $b = 1$ (or equivalently 3, given the degeneracy) interacts with the mode of acoustic origin and generates an EP. This is because modes associated with different Bloch-wave numbers are orthogonal [30]. Because both modes of acoustic origin are azimuthal modes of order $m = 1$, thus associated with Bloch-wave numbers $b = 1$, only the modes of ITA origin associated with the latter Bloch-wave numbers can interact with them and lead to the formation of EPs, or more generally to mode veering. This also explains why the ITA modes found in the clustered region do not interact with each other and neither exhibit veering nor form EPs despite their eigenvalues being so closed.

5. Conclusions

In this study, a different perspective to the notion of intrinsic modes has been presented, with the aim of associating each thermoacoustic mode with a unique origin without altering the acoustic state (in particular the reflection coefficients) of the system. We have demonstrated that this is not possible with the traditional definitions of acoustic and intrinsic modes, because these definitions are based on two separate parameters: the former are defined in the absence of heat release dynamics, when $n = 0$, whereas the latter are defined in anechoic conditions, when $R = 0$. Instead, we propose to use only one parameter, chosen to be n, to define the origin of all the modes independent of the acoustic boundary conditions of the system. We have shown in a rather general way that any thermoacoustic mode can be uniquely associated with one of these two classes of modes when $n \to 0$. Furthermore, an explicit expression has been found for the modes of ITA origin when an $n - \tau$ model is adopted. These are independent of the acoustic properties even for systems which, despite having anechoic boundary conditions, still have an acoustic response due to, e.g., area expansions. Their expressions are functions only of the coefficients of the scattering matrix $\mathbf{S}$ and the heat release scaling coefficients. In some special cases (absence of mean flow and cross-sectional area variations across the flame, anechoic boundary conditions), the definition of ITA modes proposed in this study coincides with that found in the literature for anechoic conditions. We have also discussed how, in the case of rotationally symmetric annular combustors, modes of ITA origin tend to form clusters of eigenvalues in the limit $n \to 0$, and generally behave as (weakly) coupled oscillators for finite values of n.

The presented theory enables us to theoretically estimate the location of *all* thermoacoustic eigenvalues in the limit $n \to 0$, in a given range of eigenfrequencies. The estimate is based on the numerical identification of eigenvalues of acoustic origin, found in the vicinity of acoustic modes and easily obtainable with standard Helmholtz solvers, and eigenvalues of ITA origin, in the vicinity of theoretically estimated values having large negative growth rates. Having at hand the solutions in the limit $n \to 0$, continuation methods can be used to track the trajectories of these eigenvalues to any desired value of n. This reduces the numerical effort needed for identifying large sets of thermoacoustic eigenvalues, and increases the confidence that all modes in a given frequency range have been identified. For finite values of n, the modes of acoustic and ITA origin may interact, giving rise to strong veering of the eigenvalue trajectories. This effect has been related to the existence of exceptional points (EPs) in the spectra of thermoacoustic systems, at which eigenvalues and their corresponding eigenfunctions coalesce. Even though the identified EPs always have negative growth rates, we have demonstrated how mode veering in their vicinity is responsible for strong changes in the eigenvalues sensitivities: in some cases, this can cause eigenvalues that are predicted to stabilize by linear stability analysis (for weak flames) to become unstable. In this respect, EPs can be considered as one of the causes of thermoacoustic instabilities, and their identification is practically relevant. A numerical method for the identification of real-valued EPs has been presented, which uses the self-orthogonality property of the defective eigenvalues found at EPs.

All the theoretical results presented have also been demonstrated numerically on 3D axial and annular thermoacoustic configurations. The theoretical predictions on the locations of the modes of ITA origin agree well with numerical results in all tested cases. Clustering of modes is predicted and observed in annular configurations. EPs have been identified in all configurations and can result from the interaction of (i) modes of acoustic and of intrinsic origin, or (ii) modes of only acoustic origin. No EPs resulting from the interaction between two intrinsic modes have been identified so far. The modeshapes of the EPs contain a strong signature of which modes are responsible for their formation. We have linked the existence of EPs to the topological behavior of the eigenvalue trajectories in parameter space, and related those to regimes that have been previously indicated as "weakly" or "strongly" coupled, as well as identified a new regime which is triggered at moderatly high values of the interaction index n. Generally, knowledge on the EPs' locations leads to the identification of several regimes within which the topological behavior of eigenvalue trajectories is preserved, and to a good qualitative prediction and understanding of the eigenvalue trajectories of thermoacoustic systems in parameter space.

Acknowledgments

A. Orchini is grateful to the Alexander von Humboldt Foundation for financial support via their PostDoctoral Research Fellowship.

Appendix A. Poles of the closed thermoacoustic feedback loop when $|ne^{-s\tau}| \to \mathcal{O}(1)$ for $n \to 0$

Given the expression for the growth rate (12), all the propagation terms $P_j = e^{-s\tau_j}$ diverge to infinity in the limit $n \to 0$. To find the poles of (11) when the growth rate σ becomes infinitely negative, it is convenient to rewrite it as

$$\hat{u} = \frac{1}{\frac{D(s)}{N(s)} - \mathcal{F}(s)} \hat{q}_n. \tag{A.1}$$

The fraction at the denominator of the above equation is an indeterminate form in the $\sigma \to -\infty$ limit. To solve it, we divide numerator and denominator of Eq. (7) by $P_1P_2P_3P_4$, obtaining

$$\frac{D(s)}{N(s)} = \frac{P_2^{-1}P_3^{-1}R_1S_{21}+P_1^{-1}P_4^{-1}R_2S_{12}+R_1R_2(S_{22}S_{11}-S_{21}S_{12})-(P_1P_2P_3P_4)^{-1}}{(P_1^{-1}P_4^{-1}-R_1)[P_2^{-1}P_3^{-1}H_2+R_2(H_1S_{22}-H_2S_{12})]}. \quad \text{(A.2)}$$

Considering now the limit $\sigma \to -\infty$, all the terms containing P_j^{-1} vanish because of the growth rate expression (12). Thus, Eq. (A.2) reduces to

$$\lim_{\sigma \to 0} \frac{D(s)}{N(s)} = -\frac{\cancel{R_1 R_2}(S_{22}S_{11} - S_{21}S_{12})}{\cancel{R_1 R_2}(H_1S_{22} - H_2S_{12})} \equiv -\beta, \quad \text{(A.3)}$$

where we have defined the factor β as a function of the scattering matrix elements S_{ij} and the scaling factors between flame and acoustic responses H_i. Note that the reflection coefficients, which generally include also possible area variations in the regions upstream/downstream of the flame, simplify in the above expressions.

The poles of (A.1) in the limit of infinitely negative growth rate are therefore given by

$$\frac{1}{\beta}\mathcal{F}(s) + 1 = 0. \quad \text{(A.4)}$$

The latter equation can always be solved numerically, for arbitrary expressions of the FTF. In the special case in which the flame response can be modelled with an $n - \tau$ model, $\mathcal{F}(s) = ne^{-s\tau}$, analytical solutions can be found:

$$s = \frac{1}{\tau}\log\left(\frac{n}{\beta}\right) + \frac{(2k+1)\pi}{\tau}\mathrm{i}, \qquad k \in \mathbb{Z}. \quad \text{(A.5)}$$

The angular frequencies of these solutions are identical to those of the intrinsic ones, as per Eq. (5). The expression for the growth rate is consistent with that obtained in the asymptotic limit (see Eq. (12)), with $\alpha = \beta$, which makes the solutions valid. In the special case in which no mean flow effects are considered, it can be proven that $\beta = \frac{1}{H_2}$, so that the dispersion relation (A.4) is formally equivalent to that of the pure ITA modes (10), and so are the eigensolutions. This was implicitly shown in [14], but can be derived from first principles given the explicit expressions of the scattering matrix elements.

In summary, we have proven that there always exists a set of modes in the $n \to 0$ limit which are infinitely damped, and whose frequencies are identical to those of the pure ITA modes, which are found when the reflection coefficients are set to zero.

References

[1] M. Hoeijmakers, V. Kornilov, I. Lopez Arteaga, P. de Goey, H. Nijmeijer, Intrinsic instability of flame-acoustic coupling, Combustion and Flame 161 (2014) 2860–2867.

[2] M. Hoeijmakers, V. Kornilov, I. Lopez Arteaga, P. de Goey, H. Nijmeijer, Flame dominated thermoacoustic instabilities in a system with high acoustic losses, Combustion and Flame 169 (2016) 209–215.

[3] T. Emmert, S. Bomberg, W. Polifke, Intrinsic thermoacoustic instability of premixed flames, Combustion and Flame 162 (2015) 75–85.

[4] S. Bomberg, T. Emmert, W. Polifke, Thermal versus acoustic response of velocity sensitive premixed flames, Proceedings of the Combustion Institute 35 (2015) 3185–3192.

[5] Y. Aurégan, R. Starobinski, Determination of acoustical energy dissipa-

tion/production potentiality from the acoustical transfer functions of a multiport, Acta Acustica 85 (1999) 788–792.

[6] A. Gentemann, W. Polifke, Scattering and generation of acoustic energy by a premix swirl burner, in: ASME Turbo Expo, 2007, pp. 125–133.

[7] C. F. Silva, T. Emmert, S. Jaensch, W. Polifke, Numerical study on intrinsic thermoacoustic instability of a laminar premixed flame, Combustion and Flame journal 162 (2015) 3370–3378.

[8] E. Courtine, L. Selle, T. Poinsot, DNS of intrinsic thermoacoustic modes in laminar premixed flames, Combustion and Flame 162 (2015) 4331–4341.

[9] L. Tay-Wo-Chong, S. Bomberg, A. Ulhaq, T. Komarek, W. Polifke, Comparative validation study on identification of premixed Flame Transfer Function, Journal of Engineering for Gas Turbines and Power 134 (2012) 021502 (8 pages).

[10] L. Crocco, Theoretical studies on liquid-propellant rocket instability, in: The Combustion Institute: Tenth Symposium (International) on Combustion, 1965, pp. 1101–1128.

[11] T. Poinsot, Simulation methodologies and open questions for acoustic combustion instability studies, in: Center for Turbulence Research Annual Research Briefs, 2013, pp. 179–188.

[12] C. F. Silva, M. Merk, T. Komarek, W. Polifke, The contribution of intrinsic thermoacoustic feedback to combustion noise and resonances

of a confined turbulent premixed flame, Combustion and Flame 182 (2017) 269–278.

[13] T. Emmert, S. Bomberg, S. Jaensch, W. Polifke, Acoustic and intrinsic thermoacoustic modes of a premixed combustor, in: Proceedings of the Combustion Institute, Vol. 36, 2017, pp. 3835–3842.

[14] N. K. Mukherjee, V. Shrira, Intrinsic flame instabilities in combustors: Analytic description of a 1-D resonator model, Combustion and Flame 185 (2017) 188–209.

[15] N. Hosseini, V. N. Kornilov, I. Lopez Arteaga, W. Polifke, O. J. Teerling, L. P. H. de Goey, Intrinsic thermoacoustic modes and their interplay with acoustic modes in a Rijke burner, International Journal of Spray and Combustion Dynamics 10 (2018) 315–325.

[16] W. D. Heiss, The physics of exceptional points, Journal of Physics A: Mathematical and Theoretical 45 (2012) 444016 (11pp).

[17] M. Miri, A. Alù, Exceptional points in optics and photonics, Science 363 (2019) eaar7709 (11 pages).

[18] C. Bourquard, N. Noiray, Stabilization of acoustic modes using Helmholtz and Quarter-Wave resonators tuned at exceptional points, Journal of Sound and Vibration 445 (2019) 288–307.

[19] G. A. Mensah, L. Magri, C. F. Silva, P. E. Buschmann, J. P. Moeck, Exceptional points in the thermoacoustic spectrum, Journal of Sound and Vibration 433 (2018) 124–128.

[20] A. P. Dowling, S. R. Stow, Acoustic analysis of gas turbine combustors, Journal of Propulsion and Power 19 (2003) 751–764.

[21] F. E. C. Culick, Unsteady motions in combustion chambers for propulsion systems, AGARDograph, RTO AG-AVT-039, 2006.

[22] T. Poinsot, D. Veynante, Theoretical and numerical combustion, 2nd Edition, R T Edwards, 2005.

[23] F. Nicoud, L. Benoit, C. Sensiau, T. Poinsot, Acoustic modes in combustors with complex impedances and multidimensional active flames, AIAA Journal 45 (2007) 426–441.

[24] F. E. C. Culick, Nonlinear behavior of acoustic waves in combustion chambers - l, Acta Astronautica 3 (1976) 715–734.

[25] B. E. Courtine, L. Selle, F. Nicoud, W. Polifke, C. Silva, M. Bauerheim, Causality and intrinsic thermoacoustic instability modes, in: Center for Turbulence Research, 2014, pp. 169–178.

[26] C. F. Silva, K. J. Yong, L. Magri, Thermoacoustic modes of quasi- one-dimensional combustors in the region of marginal stability, Journal of Engineering for Gas Turbines and Power 141 (2019) 021022 (8 pages).

[27] A. P. Dowling, Nonlinear self-excited oscillations of a ducted flame, Journal of Fluid Mechanics 346 (1997) 271–290.

[28] W. Polifke, Combustion instabilities, in: J. Anthoine, A. Hirschberg (Eds.), Advances in Aeroacoustics and Applications, Von Karman Institute, 2004, pp. 1–44.

[29] A. Orchini, S. J. Illingworth, M. P. Juniper, Frequency domain and time domain analysis of thermoacoustic oscillations with wave-based acoustics, Journal of Fluid Mechanics 775 (2015) 387–414.

[30] G. Mensah, L. Magri, A. Orchini, J. Moeck, Effects of asymmetry on thermoacoustic modes in annular combustors: a higher-order perturbation study, J. Eng. Gas Turbines Power 141 (2018) 041030 (8 pages).

[31] S. R. Stow, A. P. Dowling, Low-Order modelling of thermoacoustic limit cycles, in: Proceedings of ASME Turbo Expo, 2004, pp. GT2004–54245.

[32] B. Semlitsch, A. Orchini, A. P. Dowling, M. P. Juniper, G-equation modelling of thermoacoustic oscillations of partially premixed flames, International Journal of Spray and Combustion Dynamics 9 (2017) 260–276.

[33] M. Juniper, Sensitivity analysis of thermoacoustic instability with adjoint helmholtz solvers, Physical Review Fluids 3 (2018) 110509.

[34] B. Schuermans, V. Bellucci, C. O. Paschereit, Thermoacoustic modeling and control of multi burner combustion systems, in: ASME Turbo Expo, 2003, pp. GT–38688 (11 pages).

[35] A. Orchini, G. A. Mensah, J. P. Moeck, Effects of nonlinear modal interactions on the thermoacoustic stability of annular combustors, Journal of Engineering for Gas Turbines and Power 141 (2018) 021002 (10 pages).

[36] G. J. Tee, Eigenvectors of block circulant and alternating circulant matrices, New Zealand Journal of Mathematics 36 (2007) 195–211.

[37] G. A. Mensah, G. Campa, J. P. Moeck, Efficient Computation of Thermoacoustic Modes in Industrial Annular Combustion Chambers Based on Bloch-Wave Theory, Journal of Engineering for Gas Turbines and Power 138 (2016) 081502 (7 pages).

[38] P. J. Schmid, M. F. de Pando, N. Peake, Stability analysis for n-periodic arrays of fluid systems, Physical Review Fluids 2 (2017) 113902.

[39] C. Pierre, E. H. Dowell, Localization of vibrations by structural irregularity, Journal of Sound and Vibration 114 (1987) 549–564.

[40] G. Ghirardo, C. D. Giovine, J. P. Moeck, M. R. Bothien, Thermoacoustics of Can-Annular Combustors, Journal of Engineering for Gas Turbines and Power 141 (2019) 011007 (10 pages).

[41] P. E. Buschmann, G. A. Mensah, F. Nicoud, J. P. Moeck, Solution of thermoacoustic eigenvalue problems with a non-iterative method, in: ASME Turbo Expo, 2019, pp. GT2019–90834 (15 pages).

[42] A. P. Seyranian, O. N. Kirillov, A. A. Mailybaev, Coupling of eigenvalues of complex matrices at diabolic and exceptional points, Journal of Physics A: Mathematical and General 38 (2005) 1723–1740.

[43] L. Magri, M. P. Juniper, Sensitivity analysis of a time-delayed thermoacoustic system via an adjoint-based approach, Journal of Fluid Mechanics 719 (2013) 183–202.

[44] A. Orchini, M. P. Juniper, Linear stability and adjoint sensitivity analysis of thermoacoustic networks with premixed flames, Combustion and Flame 165 (2016) 97–108.

[45] R. Mennicken, M. Möller, Non-self-adjoint boundary eigenvalue problems, Elsevier, 2003.

[46] P. Luchini, A. Bottaro, Adjoint equations in stability analysis, Annual Review of Fluid Mechanics 46 (2014) 493–517.

[47] N. Moiseyev, Non-Hermitian quantum mechanics, Cambridge University Press, 2011.

[48] E. Narevicius, P. Serra, N. Moiseyev, Critical phenomena associated with self-orthogonality in non-Hermitian quantum mechanics, Europhysics Letters 62 (2003) 789–794.

[49] M. P. Juniper, R. I. Sujith, Sensitivity and nonlinearity of thermoacoustic oscillations, Annual Review of Fluid Mechanics 50 (2018) 661–689.

[50] F. Sogaro, P. Schmid, A. Morgans, Sensitivity analysis of thermoacoustic instabilities, in: International Congress on Sound and Vibration, 2018, pp. 2063–2070.

[51] C. F. Silva, W. Polifke, Non-dimensional groups for similarity analysis of thermoacoustic instabilities, Proceedings of the Combustion Institute 37 (2019) 5289–5297.

[52] M. Bauerheim, F. Nicoud, T. Poinsot, Progress in analytical methods to predict and control azimuthal combustion instability modes in annular chambers, Physics of Fluids 28 (2016) 021303.

[53] M. Bauerheim, A. Ndiaye, P. Constantine, S. Moreau, F. Nicoud, Sym-

metry breaking of azimuthal thermoacoustic modes: the UQ perspective, Journal of Fluid Mechanics 789 (2016) 534–566.

[54] T. Komarek, W. Polifke, Impact of swirl fluctuations on the flame response of a perfectly premixed swirl burner, Journal of Engineering for Gas Turbines and Power 132 (2010) 061503 (7 pages).

[55] M. A. Macquisten, M. Whiteman, S. R. Stow, A. J. Moran, Exploitation of measured Flame Transfer Functions for a two- phase lean fuel injector to predict thermoacoustic modes in full annular combustors, in: ASME Turbo Expo, 2014, pp. GT2014–25036.

[56] M. Bauerheim, J. F. Parmentier, P. Salas, F. Nicoud, T. Poinsot, An analytical model for azimuthal thermoacoustic modes in an annular chamber fed by an annular plenum, Combustion and Flame 161 (2014) 1374–1389.

[57] M. R. Bothien, N. Noiray, B. Schuermans, Analysis of azimuthal thermoacoustic modes in annular gas turbine combustion chambers, Journal of Engineering for Gas Turbines and Power 137 (2015) 061505.

[58] G. Ghirardo, M. P. Juniper, M. R. Bothien, The effect of the flame phase on thermoacoustic instabilities, Combustion and Flame 187 (2018) 165–184.

[59] K. Ding, G. Ma, M. Xiao, Z. Q. Zhang, C. T. Chan, Emergence, coalescence, and topological properties of multiple exceptional points and their experimental realization, Physical Review X 6 (2016) 021007.